Available online at www.sciencedirect.com
ScienceDirect
Catalysis Today 117 (2006) 90–97
CATALYSIS TODAY
www.elsevier.com/locate/cattod

Surface-nitrogen removal in NO reduction on Pd(1 1 0) and its retardation by oxygen: Angle-resolved desorption studies

Yunsheng Ma, Tatsuo Matsushima *

Catalysis Research Center, Hokkaido University, Sapporo 001-0021, Japan

Available online 23 June 2006

Abstract

An oxygen retarding effect toward surface-nitrogen removal processes was studied in the course of the catalyzed NO reduction on Pd(1 1 0) by angle-resolved product desorption analysis combined with cross-correlation time-of-flight techniques. Three surface-nitrogen removal processes, i.e., (i) $2N(a) \rightarrow N_2(g)$, (ii) $N(a) + NO(a) \rightarrow N_2O(a) \rightarrow N_2(g) + O(a)$ and (iii) $N_2O(a) \rightarrow N_2O(g)$ are operative when CO is a counter-reducing reagent. Process (i) becomes predominant above ca. 600 K and is most sensitively retarded by O(a). Below ca. 550 K, processes (ii) and (iii) remove most of the surface nitrogen. By addition of O(a), process (iii) is enhanced once, suggesting an increase in the amount of the intermediate $N_2O(a)$, whereas its decomposition in process (ii) is more quickly retarded.

Keywords: Nitrogen oxide; Nitrous oxide; Palladium; Single crystal surfaces; Reduction; Desorption

1. Introduction

The catalytic removal of nitrogen oxides from automobile exhaust has been achieved without definite knowledge of the reaction mechanism [1]. A deep insight into the reaction mechanism will make it possible to improve the catalysts for future generations. In this deNOx process on the best catalyst metals of rhodium and palladium, the oxygen effect to surface-nitrogen removal steps is still unclear because of the presence of several fast pathways after slow NO dissociation, i.e., the ordinary kinetic study at the steady-state NO reduction is not informative on these steps [2]. This paper delivers the first analysis of the oxygen retardation effect toward these nitrogen removal steps on Pd(1 1 0) using angle-resolved (AR) product desorption analysis. Three nitrogen removal processes change in different ways when the amount of surface oxygen increases.

Product desorption from catalyst surfaces must be consistently characterized from both chemical kinetics and reaction dynamics as performed in gas phase reactions [3]. Kinetics is concerned with the desorption frequency (reaction rate) and dynamics deals with the energy partition during an event [4]. The former is obscured by the slowest step. On the other hand, AR-product desorption analysis in the latter category is informative toward the surface-nitrogen removal processes in the course of catalyzed NO reduction whenever any step becomes rate-determining because the angular distribution does not involve the reaction rate and is always related to the desorption process [4]. Deposited surface-oxygen is removed as CO_2 when CO is used as reducing reagent. Fortunately, the surface-nitrogen removal processes on palladium yield different angular distributions of desorbing products, i.e., normally directed N_2 desorption takes place in the nitrogen associative process (i) $2N(a) \rightarrow N_2(g)$ [5,6]. Highly inclined N_2 desorption is induced in the intermediate N_2O decomposition process (ii) $NO(a) + N(a) \rightarrow N_2O(a) \rightarrow N_2(g) + O(a)$ [2]. N_2O desorption follows a broad cosine distribution in process (iii) $N_2O(a) \rightarrow N_2O(g)$ [7]. The removal of surface nitrogen as NH_3 is significant when the hydrogen pressure exceeds about half of that of NO [8].

The oxygen effect on the NO + CO reaction has frequently been reported on Pd and Rh surfaces, but the surface-nitrogen removal processes have not been analyzed. Graham et al. studied this effect on Pd(1 0 0) by monitoring the total CO_2 signal [9]. The addition of O_2 increased the CO_2 formation rate below $T_S = 500$ K but had almost no effect on the rate of NO reduction. The formation rates of N-containing products (N_2 and N_2O) were insensitive to the presence of oxygen. Permana

* Corresponding author. Tel.: +81 11 706 9120; fax: +81 11 706 9120.
E-mail address: tatmatsu@cat.hokudai.ac.jp (T. Matsushima).

0920-5861/$ – see front matter © 2006 Published by Elsevier B.V.
doi:10.1016/j.cattod.2006.05.004

et al. also reported that the CO_2 production rate was increased by a factor of about 4 by the addition of oxygen on Rh(1 1 1) [10]. However, Zaera and his co-workers, using effusive molecular beams, showed that the addition of oxygen suppressed not only the NO reduction but also the CO oxidation on Rh(1 1 1) [11]. In fact, these observations were mostly reproduced under slightly different conditions in the present work.

A combination of the angular and velocity distributions provides the analysis of most of the elementary processes involved in this catalyzed reaction [2]. These distributions were frequently analyzed in this catalyzed reaction with relaxation methods to avoid the large N_2 formation on the chamber wall [6,12,13] and obtain kinetic information of the fast nitrogen removals [14]. Steady-state conditions, however, cannot be established for the reaction. In the present work, AR-product desorption was successfully analyzed for the steady-state NO + CO + O_2 reaction. Process (i) is most sensitively retarded by O(a). By addition of O(a), process (iii) is enhanced once, whereas process (ii) is more quickly retarded.

2. Experiments

The apparatus with three chambers was previously described [4,7]. Briefly, the reaction chamber is equipped with X-ray photoelectron spectroscopy (XPS) optics, low-energy electron diffraction (LEED), an ion gun and a quadrupole mass spectrometer (QMS) for angle-integrated (AI) measurements. The chopper house, which has a large pumping rate of about 7 $m^3\ s^{-1}$ for high angle resolution [15], has a narrow slit facing

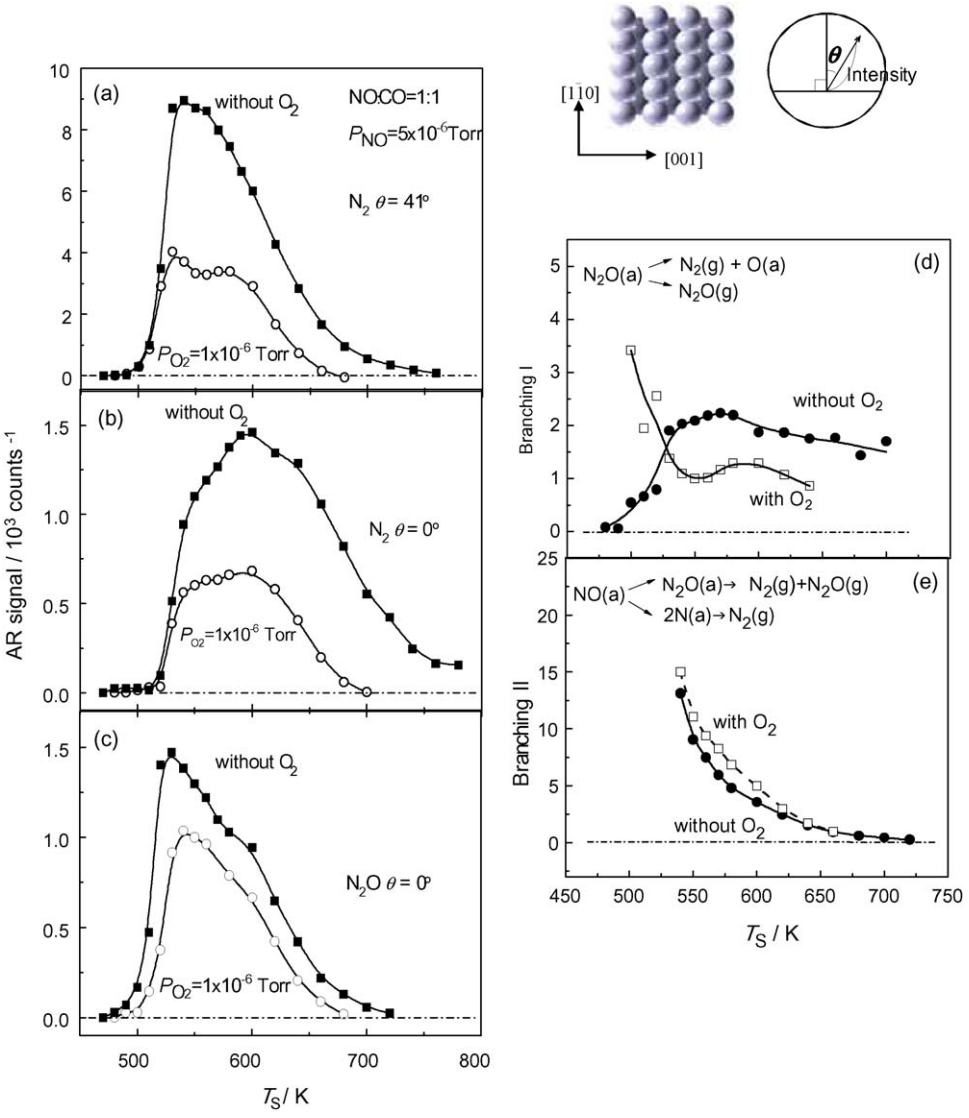

Fig. 1. Surface temperature dependence of the AR-nitrogen-containing product signals at their collimation angles and the branching ratios in nitrogen removal in a steady-state $^{15}NO + CO$ reaction. (a) $^{15}N_2$ at 41° off the surface normal toward the [0 0 1] direction. (b) $^{15}N_2$ at the surface normal and (c) $^{15}N_2O$ at the normal direction. The closed symbols show the results when the ^{15}NO pressure was 5×10^{-6} Torr and the pressure ratio of $^{15}NO/CO$ was unity. The open circles show the signals when the pressure ratio of $^{15}NO:CO:O_2 = 1:1:0.2$. Branching ratios of surface-nitrogen removal vs. temperature; (d) [inclined N_2 emission]/[N_2O] and (e) {[inclined N_2 emission] + [N_2O]}/{[normally directed N_2 emission] + [cosine N_2 emission]}. [] indicates the total amount of each species. Top view of Pd(1 1 0), its crystal azimuths, the desorption angle θ and the intensity presentation are drawn on the top.

the reaction chamber and a cross-correlation chopper blade [16]. Another QMS was set in the analyzer connected through a tube slit for AR-product desorption and time-of-flight analyses. The distance from the ionizer to the chopper blade is 377 mm, and the selected time resolution is 20 μs. This apparatus provides angle-resolved product desorption measurements without disturbing the steady-state catalyzed reaction condition. ^{15}NO (or $^{15}N_2O$) was introduced through a doser with a small orifice (diameter, 0.1 mm) about 2 cm from a sample crystal, while ^{13}CO was backfilled. Hereafter, isotopes ^{15}N and ^{13}C are simply designated as N and C in the text, respectively. The desorption angle (polar angle, θ) was scanned in the plane along the [0 0 1] direction [2] (Fig. 1).

3. Results

3.1. NO + CO reaction

The steady-state NO + CO reaction becomes observable above 500 K with a maximum rate at about 550 K. In Fig. 1, the

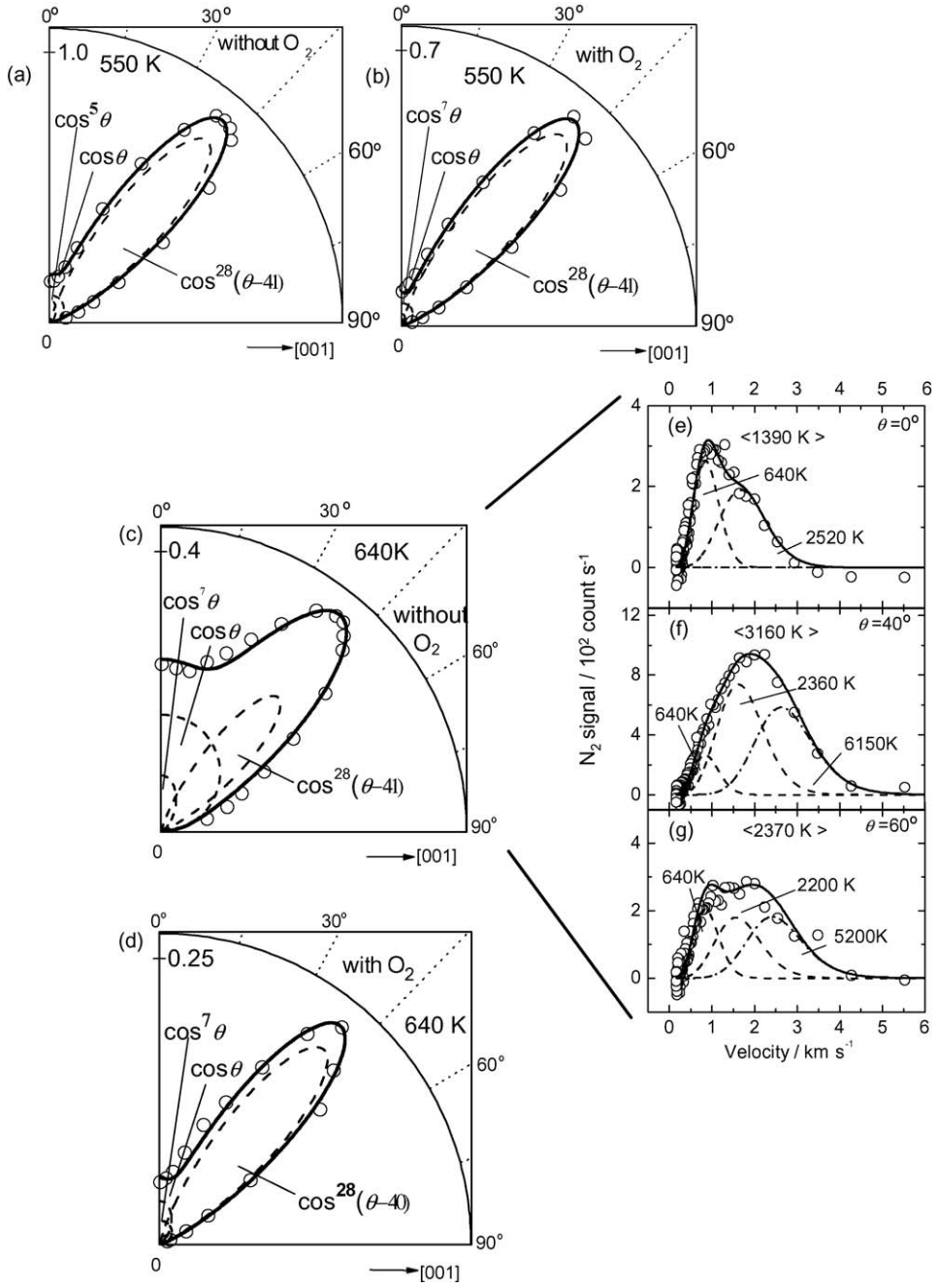

Fig. 2. Angular (a–d) and velocity (e–g) distributions of desorbing $^{15}N_2$ in the steady-state $^{15}NO + CO$ reaction. (a) 550 K, $P_{NO} = 5 \times 10^{-6}$ Torr with a ratio of $^{15}NO/^{12}CO = 1$ and (b) O_2 was added to 1×10^{-6} Torr. (c) 640 K, $P_{NO} = 5 \times 10^{-6}$ Torr with a ratio of $^{15}NO/^{12}CO = 1/2$, and (d) $P_{NO} = P_{CO} = 5 \times 10^{-6}$ Torr, $P_{O_2} = 1 \times 10^{-6}$ Torr. (e–g) 640 K, $P_{NO} = 5 \times 10^{-6}$ Torr with a ratio of $^{15}NO/^{12}CO = 1/2$ at different θ values. Typical deconvolutions are given by broken curves. The solid line indicates their summation. The average kinetic energy is shown in $\langle\cdot\rangle$ in temperature units. The translational temperature of each component is also shown.

AR N_2 signal at $\theta = 41^\circ$ and 0° is shown at an equi-molar mixture of NO and CO versus the surface temperature (T_S). The AR-N_2 signal is maximized at these angles as described in the next section. Below 600 K, the N_2 signal at $\theta = 41^\circ$ is much higher than that at the normal direction and peaks at 520 K. On the other hand, the signal at the normal direction is extended to higher temperatures, showing a broad maximum at around 600 K. The AR-N_2O signal showed a similar temperature dependence to that of N_2 at 41°. The main product containing oxygen is CO_2, which is about five times more than the amount of N_2O. The ratio of $\{2[N_2] + [N_2O]\}/[CO_2]$ was confirmed to be kept at unity throughout the studied T_S, where $[N_2]$, $[N_2O]$ and $[CO_2]$ are the amount of each species estimated from their AI signals, i.e., only the reaction $(NO + CO) \rightarrow (N_2 + N_2O + CO_2)$ takes place. The product CO_2 sharply collimates along the surface normal as a $(\cos\theta)^{13}$ form that is very similar to that in the $CO + O_2$ reaction [17]. Only the (1×1) pattern was observed in LEED measurements under a steady-state CO + NO reaction at the total pressure of 1×10^{-7} Torr of the equi-molar mixture of NO and CO in the range of 400–800 K. It shows that the surface is under reducing conditions and the inclined N_2 desorption takes place on the (1×1) area, and not on the reconstructed surface [18].

The NO reduction is largely suppressed when O_2 is introduced (Fig. 1). It is noteworthy that the N_2 signal intensities at both $\theta = 0^\circ$ and 41° decrease by about 60%, whereas the N_2O signal intensity decreases by only about 30%. The surface oxygen not only suppresses the reduction rate but also changes the reaction selectivity. This will be studied from an elementary process point of view.

3.2. Desorption components

The desorption of product N_2O showed a cosine flux distribution and Maxwellian velocity distribution at the surface temperature, implying that the product N_2O is trapped on the surface prior to desorption [7]. On the other hand, the angular distribution of desorbing N_2 largely depends on the surface temperature and CO/NO pressure ratio. Below 550 K, the N_2 desorption sharply collimates at around 41° over a wide CO pressure range even in the presence of gaseous O_2 (Fig. 2(a and b)). The N_2 signal at the surface normal direction is week, indicating little contribution from the normally directed component. At higher temperatures, however, the N_2 signal at the normal direction is enhanced, especially at high CO pressures (Fig. 2(c and d)). The normally directed component is decreased in the presence of oxygen. The distribution was deconvoluted into three components based on the following velocity distribution analysis.

The velocity distributions of desorbing N_2 at different desorption angles at T_S = 640 K are shown in Fig. 2(e–g). The apparent translational temperature calculated as $T_{\langle E\rangle} = \langle E\rangle/2k$ is shown in $\langle\cdot\rangle$ in the figure, where $\langle E\rangle$ is the average kinetic energy and k is the Boltzmann constant. The value was maximized to 3160 K at around 40° and decreased with an increasing shift from the collimation angle, consistent with the inclined desorption. The velocity distribution involved the thermalized component (i.e., a Maxwellian distribution at the surface temperature) as well as that faster than that Maxwellian component. The thermalized component yields a cosine distribution in the angular distribution and was first subtracted from the velocity distribution curves. The resultant velocity curve provided the flux of the fast component, which peaked at $\theta = 0^\circ$ and 40°. The fast component yielded the maximum with a translational temperature of about 4000 K at $\theta = 40^\circ$ and showed of about 2500 K at $\theta = 0^\circ$ (Fig. 3(a)).

Assuming a power series of the cosine of the desorption angle shift from the collimation position to each component, the N_2 flux was approximated in a two-directional form as $\{\cos^{28}(\theta + 41) + \cos^{28}(\theta - 41)\}$ below 600 K (Fig. 2(a and b)). With increasing T_S above 600 K, the normally directed component was enhanced. The total signal at 640 K was approximated as $\{\cos^{28}(\theta + 41) + \cos^{28}(\theta - 41)\} + \chi(0.5\cos^5\theta + \cos\theta)$. The pre-factors indicate the relative intensity. The χ value increased at higher T_S values or higher CO/NO pressure ratios, indicating that they come from different nitrogen removal steps. The former was assigned to the decomposition of N_2O oriented along the [0 0 1] direction [2] and the latter was due to the associative desorption of N(a) [5,6]. The cosine component is involved in the latter because its kinetic behavior, i.e., its temperature dependence and CO and

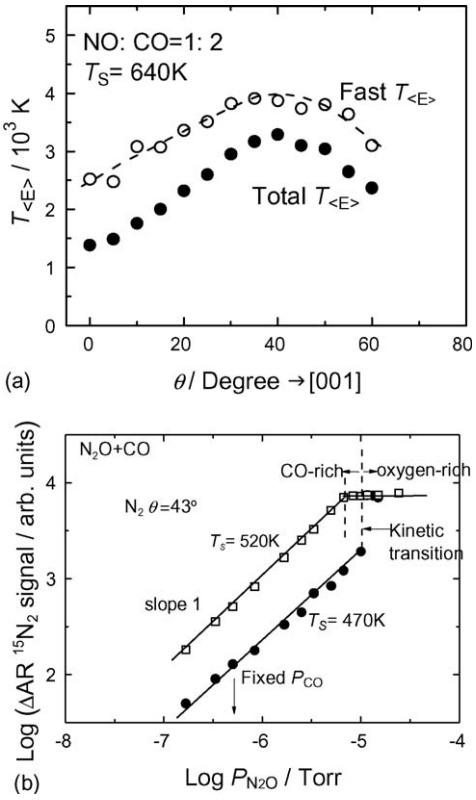

Fig. 3. (a) Angle-dependence of the translational temperature of desorbing N_2 in the plane along the [0 0 1] direction in the steady-state $^{15}NO + CO$ reaction at $P_{NO} = 5 \times 10^{-6}$ Torr with a ratio of $^{15}NO/^{12}CO = 1/2$. T_S = 640 K. "Fast $T_{\langle E\rangle}$" indicates the translational temperature after subtraction of the thermalized component. (b) N_2O pressure dependence of its reduction with CO at 520 K and 470 K. $P_{CO} = 5 \times 10^{-7}$ Torr. The surface sharply switches as shown by the vertical broken lines to oxygen-rich conditions at a critical pressure of $P_{N_2O} \gg P_{CO}$.

NO pressure dependence, is similar to those of the normally directed N_2 desorption [8]. This is also supported by the lack of the thermalized N_2 component in a steady-state $N_2O + CO$ reaction on Pd(1 1 0) in the range of 450–800 K as described below. Of course, the thermalized component cannot be assigned to a definite process from the angular distribution.

The steady-state $N_2O + CO$ reaction proceeded above around 450 K at $P_{CO} = 0.5 \times 10^{-6}$ Torr. This starting temperature shifted to around 400 K at lower P_{CO}. It is determined by the CO(a) removal because N_2O(a) is dissociated below 160 K [19] and the reaction of deposited O(a) with CO(a) is very fast [4]. The N_2 formation increased steeply with increasing T_S, reached a maximum at around 500 K and then decreased at higher T_S values. The product CO_2 desorption sharply collimated along the surface normal. The N_2 desorption collimated in a very similar way to that in the NO + CO reaction below 550 K. The angular distribution became broader at high temperatures from a $\cos^{28}(\theta - 45)$ form at 410 K to a $\cos^{19}(\theta - 46)$ form at 750 K. Desorbing N_2 showed translational temperatures in the range of 2000–5000 K, similar to those in the NO + CO reaction below 550 K. Neither the cosine distribution nor the Maxwellian velocity distribution component at the surface temperature was found in desorbing N_2 in the N_2O reduction [20].

The reaction kinetics was switched at a critical N_2O/CO pressure ratio, 12–30, depending on the surface temperature. Below this point, the reaction is a first order in N_2O and negative orders in CO (Fig. 3b). Above the critical point, the reaction is insensitive to N_2O and a first order in CO. The reaction shows a switching of the rate-determining step from N_2O adsorption to CO adsorption at the critical point in similar fashion to that in CO oxidation [4], where the surface is covered by CO above the critical CO pressure and by O(a) below the critical point [21]. However, no changes were found in the angular and velocity distributions of desorbing N_2 below and above the critical point. This suggests that the N_2O decomposition proceeds on clean parts. In fact, the N_2O decomposition is highly suppressed by pre-adsorbed oxygen [19,22].

3.3. Oxygen effect in NO + CO reaction

The addition of oxygen changes the CO_2 and N_2 formation rates in different ways, but the angular distributions of desorbing products remain invariant. The results at $T_S = 550$ K ($P_{NO}/P_{CO} = 1/2$ at $P_{NO} = 5 \times 10^{-6}$ Torr) are shown in Fig. 4(a), where the AR signals are shown as a function of the oxygen pressure (P_{O_2}). With increasing P_{O_2}, the total CO_2 formation is greatly enhanced initially, and then decreases. The behavior of N_2 and N_2O formation, on the other hand, is quite different. The AR-N_2 signal at 40° first increases slowly and decreases steeply above $P_{O_2} = 2 \times 10^{-6}$ Torr. This point, which indicates the starting of the retardation of step (ii), is named Point (1). The AR-N_2 signal at the surface normal slowly decreases from the beginning (immediately after O_2 addition), indicating the most sensitive toward oxygen accumulation. On the other hand, the N_2O signal at the normal direction increases once and decreases above the CO_2 maximum, named as Point (2). The figure also shows the total NO reduction rate (ΔNO) estimated from the AR-signals of N_2 and N_2O at 0° and N_2 at 40° [23]. It remains invariant below Point (1). Between Points (1) and (2), the suppression of NO reduction mostly affects the inclined N_2 emission. Above Point (2), the rate of CO oxidation using gaseous O_2 decreases quickly and reaches a steady level at Point (3) where the NO reduction is completely suppressed. The associative desorption of N(a), yielding the normally directed desorption, slowly decreases all the way.

These oxygen effects are similar at different NO/CO pressure ratios and surface temperatures. The region below Point (1) is

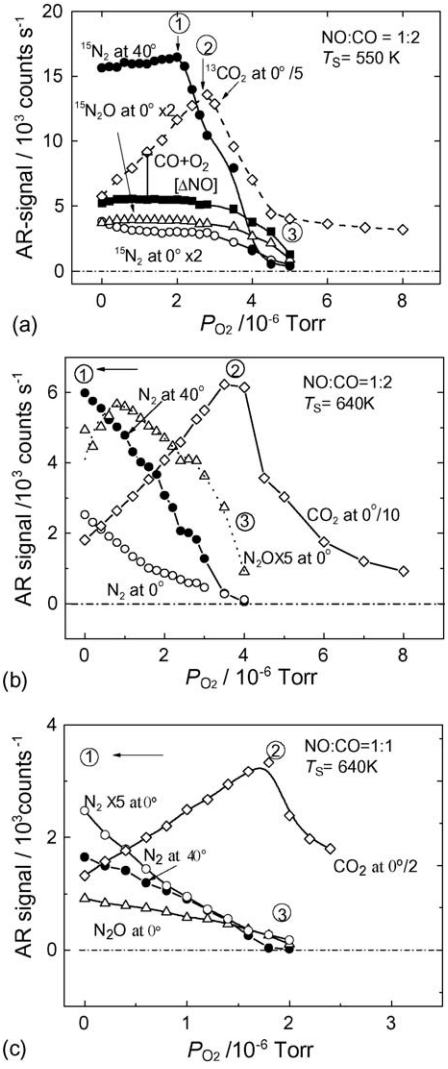

Fig. 4. P_{O_2} dependence of the AR-product signals at their collimation angles in the steady-state $^{15}NO + {}^{12}CO$ reaction at $P_{NO} = 5 \times 10^{-6}$ Torr. (a) $T_S = 550$ K and $P_{NO}/P_{CO} = 1/2$. (b) $T_S = 640$ K and $P_{NO}/P_{CO} = 1/2$. (c) $T_S = 640$ K and $P_{NO}/P_{CO} = 1$. Typical kinetic critical points marked by 1, 2 and 3 show the starting of the retardation of the inclined N_2 emission, that of the CO_2 formation and the complete suppression of the NO reduction, respectively. It should be noted that each process shows different dependence. "[ΔNO] indicates the total NO reduction rate, which was estimated from the AR-N_2 at 40°and 0° and N_2O at 0° signals and their angular distributions, was normalized to the CO_2 signal sensitivity so that the stoichiometry could be examined for the reaction $NO + CO \rightarrow N_2 + N_2O + CO_2$. The vertical bar indicates the contribution from the $CO + O_2$ reaction to the CO_2 formation.

suppressed when the initial NO/CO pressure ratio is higher or the surface temperature is higher, indicating that the surface is already covered by oxygen to a level retarding the inclined N_2 desorption. The results at 640 K are shown in Fig. 4(b and c). At $P_{NO}/P_{CO} = 0.5$, the N_2O signal once increases and decreases. When P_{NO}/P_{CO} is increased to 1, the N_2O signal as well as the N_2 signals at 40° and 0° decrease with increasing oxygen. The results at 550 K and $P_{NO} = 5 \times 10^{-6}$ Torr ($P_{NO}/P_{CO} = 1$) are similar to those at 640 K. At higher temperatures, the region between Points (1) and (2) is extended.

4. Discussion

4.1. Reaction pathways

The product N_2 is commonly emitted from N_2O(a) oriented along the [0 0 1] direction in both NO + CO and N_2O + CO reactions below about 550 K. In the steady-state NO + CO + O_2 reaction, the angular and velocity distributions of the products are very similar to those in the NO + CO reaction, i.e., the reaction pathways do not change by the addition of oxygen. The surface-nitrogen removal processes are likely to proceed on vacant parts (not on oxygen-covered sites). NO(a) dissociation is highly retarded by the addition of O(a). The resultant reduced amount of N(a) decreases the rates of the surface-nitrogen removal processes in different ways.

This mechanism with intermediate N_2O has frequently been proposed; however, the N_2O formation has not been recognized in the main surface-nitrogen removal process to N_2 and rather treated as one of the side reactions not emitting N_2. This is because the intermediate N_2O(a) has not been confirmed by spectroscopic methods in the course of the catalyzed NO reduction [24], and no direct evidence emitting N_2 was found until the angular distribution work was conducted [2]. In fact, the surface-parallel N_2O must be insensitive to vibrational spectroscopy according to the surface selection rule [25]. Furthermore, the standing form with the terminal nitrogen interacting with metal atoms, which was observed at around 90 K after N_2O adsorption by vibrational spectroscopy [18], is unsuitable as the precursor emitting N_2 in the inclined way. A lying form along the [0 0 1] direction as well as the standing form on the terminal nitrogen was recently proposed by density functional theory (DFT) calculations in a generalized gradient approximation [26]. These forms were later confirmed by scanning tunneling microscopy (STM) work at 14 K [27] and near-edge X-ray absorption fine-structure (NEXAFS) work at around 60 K [28]. In the course of catalyzed NO reduction, the population of the lying form of N_2O must be greater than the alternative because of its slightly higher heat of adsorption [26]. Fortunately, its decomposition emits N_2 in a peculiar way, making its identification possible in the desorption dynamics. The contribution from the adsorption of gaseous N_2O once desorbed is less because of the much lower sticking probability, i.e., around 1/30 of that of NO or CO. The surface condition is mostly controlled by the pressure ratio of NO/CO/O_2 and the surface temperature.

Only the inclined N_2 desorption proceeds in the N_2O + CO reaction in the wide temperature range studied, 400–800 K. Therefore, the thermalized (cosine distribution) component of N_2 in the NO + CO reaction should be formed in the other processes, probably in the associative process of N(a). In the following section, process (i) is treated to yield both the normally directed and cosine N_2 components. In the N_2O dissociation, fragment N_2 is repulsed by the nascent O(a) which is more or less negatively charged on the metal surface. High repulsive forces may be operative between the resultant bulky ionic oxygen and the leaving N_2. This scenario was already examined by DFT calculations, which predict that the main component of the reaction coordinate is along the N–O bond direction [26].

4.2. Branchings in pathways

There are three kinds of branching in surface-nitrogen removal processes involved the NO + CO reaction on Pd(1 1 0). First is the branching of the intermediate N_2O decomposition to desorption, i.e., in the conversion of N_2O(a) into N_2(g) + O(a) and N_2O(g). The branching ratio in this conversion is estimated as

$$\text{Branching I} = \frac{[\text{Inclined } N_2]}{[N_2O]} \quad (1)$$

where [inclined N_2] and [N_2O] are the amount of each species estimated from their AR-signal intensities and angular distributions [23]. The results at $P_{NO} = P_{CO} = 5 \times 10^{-6}$ Torr are shown as a function of the surface temperature in Fig. 1(d). The ratio increases with increasing temperature below 550 K and shows a constant value around 2 above it. This increase is due to the decreasing blocking by CO(a) through its removal and the activation energy of the dissociation is not necessarily higher than that of desorption. In fact, the branching ratio decreases below 550 K with increasing temperature when O_2 is introduced at 1×10^{-6} Torr. Adsorbed oxygen in a small amount can stabilize N_2O(a) [29].

Second is the branching in the conversions of N(a) formed from the NO(a) dissociation into process (i) and the N_2O(a) formation. The branching is presented by the ratio of the sum of the inclined N_2 and the cosine N_2O desorption to that of the normally directed N_2 and the cosine N_2 desorption as,

$$\text{Branching II} = \frac{\{[\text{inclined } N_2] + [N_2O]\}}{\{[\text{normally directed } N_2] + [\text{cosine } N_2]\}} \quad (2)$$

where [normally directed N_2] and [cosine N_2] were again estimated from their signal intensity and angular distributions. The ratios estimated at $P_{NO} = P_{CO} = 5 \times 10^{-6}$ Torr are shown versus temperature in Fig. 1(e). It becomes very large below 550 K, indicating that the reaction proceeds mostly through the intermediate N_2O pathways. Above 650 K, the ratio decreases below unity and process (i) becomes predominant. Third is the branching in process (i) as presented by a ratio of the normally directed N_2 to the cosine N_2 component. This is always kept at around 0.1, irrespective of the surface temperature and NO/CO pressure ratio, i.e., its product N_2 is mostly thermalized. The first two branching ratios changed in the presence of gaseous oxygen.

4.3. Oxygen effect toward each process

With increasing P_{O_2}, the total CO_2 formation is once enhanced steeply and then decreased. The CO_2 formation increases even when the oxygen supply from the NO dissociation is reduced. The amount of CO_2 receiving the O(a) supplied from adsorbed O_2 was estimated as the difference between the total CO_2 and the reduced amount of NO (ΔNO). The NO dissociation was found to be retarded by surface oxygen, whereas the sticking coefficient of O_2 dissociative adsorption remains near 0.9 up to a surface atomic oxygen coverage of approximately one third of a monolayer [30]. At T_S = 550 K, the CO_2 formation begins to decrease before the NO reduction is completely suppressed. On the other hand, at 640 K it starts to decrease around the complete suppression of NO reduction.

The oxygen effect appears in three different stages. Below Point (1), the surface oxygen content is very low because the surface is still under reducing conditions and only process (i), the associative desorption of N(a) is retarded. The amount of N(a) already starts to decrease in this region. Both the inclined N_2 emission and N_2O desorption are enhanced. The ratio of the integrated amount of the inclined N_2, the normally directed N_2 and the cosine N_2O emission was estimated to be 1.1:0.25:0.44 without oxygen at 550 K and P_{NO}/P_{CO} = 1/2 (the condition in Fig. 4(a)), i.e., about 70 % of the intermediate N_2O is decomposed. The retardation of process (ii) appears beyond Point (1) before the maximum of N_2O formation. This means that the N_2O formation is less sensitive to O(a) accumulation than its dissociation, i.e., the amount of N_2O(a) is maximized by addition of O(a) even when the inclined N_2 emission decreases smoothly. This indicates that the N_2O(a) dissociation is retarded, or the N_2O(a) formation is increased. The latter is unlikely because the amount of N(a) decreases, whereas the former is likely because of the stabilization effect by O(a) in a small amount as described below [29]. Such behavior was also observed at higher temperatures (Fig. 4(b)). The N_2O formation shows a maximum whereas the inclined N_2 desorption decreases quickly. This N_2O maximum disappears when the surface is more covered by oxygen and/or N(a).

Process (i) is the most sensitive toward surface oxygen since it involves two nitrogen atoms, i.e., a second-order reaction in N(a). It decreases from the initial addition of oxygen because of the reduced amount of N(a). Process (ii) is also sensitive to the addition of oxygen. This is expected because the N_2O decomposition is severely suppressed by co-adsorbed oxygen on Pd(1 1 0) and Rh(1 1 0) [19,22]. However, the presence of small amounts of oxygen can stabilize N_2O(a) as reported on Ru(0 0 1) [29]. The heat of adsorption of N_2O is increased on metal sites charged positively. It is induced by coordinated oxygen with a high electro-negativity. The N_2O dissociation is retarded by this effect as well as decreasing vacant sites. Thus, N_2O emission process (iii) once increases and then decreases, indicating that N_2O(a) dissociation is more retarded than its formation. Eventually, the inclined N_2 desorption process (ii) has a chance to remain nearly constant and then decreases quickly. This is a typical kinetic behavior of two first-order consecutive reactions with the intermediate. On the other hand, the CO_2 formation can increase even when the NO reduction is suppressed. It is due to the enhanced supply of surface oxygen. The CO_2 formation is not rate-determining, and the rate-determining CO adsorption is hardly reduced by O(a), except for very high coverage [31].

The oxygen effect described above becomes clearer in the branching ratio of each pathway. The branching I is shown in Fig. 5(a). The ratio always decreases with increasing P_{O_2} regardless of the temperature and the P_{NO}/P_{CO} ratio. In fact, the ratio decreases with increasing temperature in the presence of oxygen as shown in Fig. 1(d). The value at P_{NO}/P_{CO} = 1 without oxygen is larger than that at P_{NO}/P_{CO} = 1/2, i.e., the selectivity to N_2 is increased at lower P_{CO} values but decreases quickly by addition of O_2. At higher CO pressures, the surface oxygen must decrease, however, the selectivity to N_2 shifts toward lower values. This means that the CO effect is not explained by the resultant surface oxygen change alone. Adsorbed nitrogen atoms or CO(a) must affect the selectivity, for example, the N_2O(a) dissociation is retarded by CO(a) or N(a).

At higher temperatures, the contribution of process (i) becomes remarkable because of its high activation energy even in the presence of oxygen (Fig. 1(e)) [32]. The branching of the N_2O pathway to the associative process is shown as a function of O_2 pressure in Fig. 5(b). At 550 K, the NO reduction proceeds mostly through the N_2O pathway (Fig. 1d). This branching is further increased with increasing P_{O_2}. At 640 K, the ratio is close to unity, indicating a comparable contribution from both pathways. The branching ratio again increases with increasing P_{O_2}. At low O_2 pressure, the branching to N_2O pathway is enhanced by reduced process (i), whereas at high O_2 pressures,

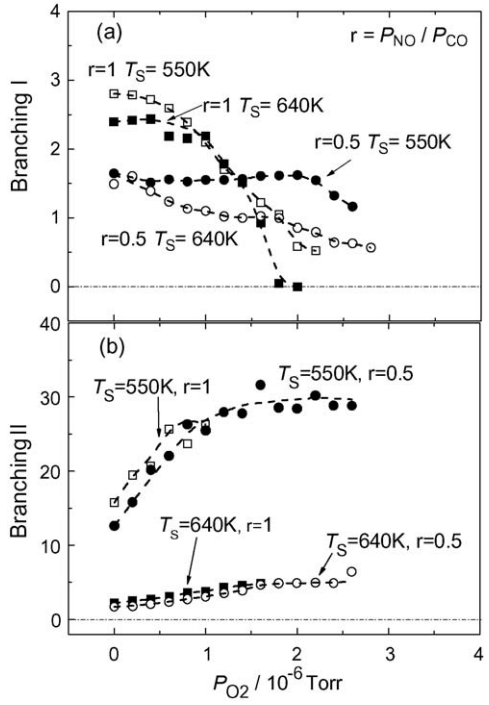

Fig. 5. Branching of surface-nitrogen removal in the NO + CO + O_2 reaction as a function of the O_2 pressure at different T_S and $r \equiv P_{NO}/P_{CO}$. (a) Ratio of [inclined N_2 emission]/[N_2O]. (b) Ratio of {[inclined N_2 emission] + [N_2O]}/{[normally directed N_2 emission] + [cosine N_2 emission]}.

the N_2O dissociation is highly retarded by oxygen, increasing the N_2O fraction. A high selectivity to N_2 through process (i) is obtained only when the O_2 pressure is very low. On the other hand, another high selectivity to N_2 can be obtained through processes (ii) and (iii) even in the presence of O_2 but in the limited range.

5. Conclusions

The branching of surface-nitrogen removal pathways was examined in the steady-state $NO + CO + O_2$ reaction on Pd(1 1 0) by angle-resolved product desorption combined with velocity distribution analysis. This method has successfully provided information on surface-nitrogen removal processes although these are not rate-determining. The results are summarized in the following.

(1) The reaction proceeds via. three surface-nitrogen removal processes even in the presence of oxygen, (i) $2N(a) \rightarrow N_2(g)$, (ii) $NO(a) + N(a) \rightarrow N_2O(a) \rightarrow N_2(g) + O(a)$ and (iii) $N_2O(a) \rightarrow N_2O(g)$.
(2) Process (i) is the most sensitively retarded by O(a). The $N_2O(a)$ dissociation is severely retarded by O(a) and the selective dissociation to N_2 is always lowered by oxygen.

Acknowledgements

The authors thank Dr. A. Kokalj (Stefan Institute) for his stimulating discussion and Ms. Hiratsuka for drawing the figures. This work was partially supported by a 1996 COE special equipment program of the Ministry of Education, Sports and Culture of Japan.

References

[1] S. Matsumoto, Catal. Today 90 (2004) 183.
[2] T. Matsushima, I.I. Rzeznicka, Y.-S. Ma, Chem. Record. 5 (2005) 81.
[3] R.D. Levine, R.B. Bernstein, Molecular Reaction Dynamics, Oxford University Press, Oxford, 1974 (Chapter 1).
[4] T. Matsushima, Surf. Sci. Rep. 52 (2003) 1.
[5] T. Matsushima, Surf. Sci. 197 (1988) L287.
[6] M. Ikai, K.I. Tanaka, J. Phys. Chem. B 103 (1999) 8277.
[7] I.I. Rzeznicka, Y.-S. Ma, G. Cao, T. Matsushima, J. Phys. Chem. B 108 (2004) 14232.
[8] Y.-S. Ma, T. Matsushima, J. Phys. Chem. B 109 (2005) 1256.
[9] G.W. Graham, A.D. Logan, M. Shelef, J. Phys. Chem. 97 (1993) 5445.
[10] H. Permana, K.Y. Simon Ng, C.H.F. Peden, S.J. Schmieg, D.K. Lambert, D.N. Belton, Catal. Lett. 47 (1997) 5.
[11] C.S. Gopinath, F. Zaera, J. Catal. 200 (2001) 270.
[12] V.I. Pârvulescu, P. Grange, B. Delmon, Catal. Today 46 (1998) 233.
[13] Y. Li, M. Bowker, Surf. Sci. 348 (1996) 67.
[14] J.I. Colonell, K.D. Gibson, S.J. Sibener, J. Chem. Phys. 104 (1996) 6822.
[15] M. Kobayashi, Y. Tuzi, J. Vac. Sci. Technol. 16 (1979) 685.
[16] G. Comsa, R. David, B.J. Schumacher, Rev. Sci. Instrum. 52 (1981) 789.
[17] Md.G. Moula, S. Wako, G. Cao, K. Kimura, Y. Ohno, I. Kobal, T. Matsushima, Phys. Chem. Chem. Phys. 1 (1999) 3677.
[18] S. Haq, A. Hodgson, Surf. Sci. 463 (2000) 1.
[19] H. Horino, S. Liu, A. Hiratsuka, Y. Ohno, T. Matsushima, Chem. Phys. Lett. 341 (2001) 419.
[20] Y.-S. Ma, I. Kobal, T. Matsushima, J. Phys. Chem. B 109 (2005) 689.
[21] Y.-S. Ma, S. Han, T. Matsushima, Langmuir 21 (2005) 9529.
[22] S. Liu, H. Horino, A. Kokalj, I. Rzeznicka, K. Imamura, Y.-S. Ma, I. Kobal, Y. Ohno, A. Hiratsuka, T. Matsushima, J. Phys. Chem. B 108 (2004) 3828.
[23] G. Cao, Md.G. Moula, Y. Ohno, T. Matsushima, J. Phys. Chem. B 103 (1999) 3235.
[24] E. Ozensoy, D.W. Goodman, Phys. Chem. Chem. Phys. 6 (2004) 3765.
[25] N.V. Richardson, N. Sheppard, in: J.T. Yates, Jr., T.E. Madey (Eds.), Vibrational Spectroscopy of Molecules on Surfaces, Plenum Press, New York, 1987, p. 1.
[26] A. Kokalj, I. Kobal, T. Matsushima, J. Phys. Chem. B 107 (2003) 2741.
[27] K. Watanabe, A. Kokalj, Y. Inokuchi, I. Rzeznicka, K. Ohshimo, N. Nishi, T. Matsushima, Chem. Phys. Lett. 406 (2005) 474.
[28] K. Watanabe, A. Kokalj, H. Horino, I. Rzeznicka, K. Takahashi, N. Nishi, T. Matsushima, Jpn. J. Appl. Phys. 45 (2006) 2290.
[29] H.H. Huang, C.S. Seet, Z. Zou, G.Q. Xu, Surf. Sci. 356 (1996) 181.
[30] J. Goschnick, M. Wolf, M. Grunze, W.N. Unertl, J.H. Block, J. Loboda-Cackovic, Surf. Sci. 178 (1986) 831.
[31] T. Engel, G. Ertl, Adv. Catal. 28 (1979) 1.
[32] D.N. Belton, C.L. DiMaggio, K.Y. Simon Ng, J. Catal. 144 (1993) 273.